Thermoanalytical properties and structure of $(As_2Se_3)_{100-x}(Sb_2Se_3)_x$ glasses by Raman and ^{77}Se MAS NMR using a multivariate curve resolution approach

E. Černošková[1], J. Holubová[3], B. Bureau[2], C. Roiland[2], V. Nazabal[2], R. Todorov[4], Z. Černošek[3]

[1]Joint Laboratory of Solid State Chemistry of IMC CAS, v.v.i., and University of Pardubice, Faculty of Chemical Technology, Studentská 84, 532 10 Pardubice, Czech Republic, eva.cernoskova@upce.cz

[2]ISCR, UMR-CNRS 6226, University of Rennes 1, France.

[3]Department of General and Inorganic Chemistry, Faculty of Chemical Technology, University of Pardubice, Studentská 573, 532 10 Pardubice, Czech Republic.

[4]Institute of Optical Materials and Technologies, Acad. G. Bonchev Str., bil. 109, 113 Sofia, Bulgaria.

Keywords: As-Sb-Se glass; DSC; StepScan DSC; Raman spectroscopy; ^{77}Se MAS NMR; local structure

Abstract

The basic thermoanalytical characteristics and structure of $(As_2Se_3)_{100-x}(Sb_2Se_3)_x$ bulk glasses over the whole glass-forming region (x = 0 – 50) were studied by DSC, StepScan DSC and both Raman and ^{77}Se MAS NMR spectroscopies. The glass transition temperature, T_g, was found to increase only slightly from 184 to 190 °C with increasing Sb_2Se_3 content, and the changes in the isobaric heat capacity at T_g are also nearly compositionally independent. However, the isobaric heat capacity of glasses decreases

because of the higher atomic mass of antimony. The undercooled melts undergo crystallization when heated; As_2Se_3 crystallizes for $x \leq 20$, and both stoichiometric triselenides crystallize for higher x.

^{77}Se MAS NMR spectroscopy was used for the first time in the structural study of this pseudobinary system. The results of both NMR and Raman spectroscopies were combined, and their chemometric analysis was used to elucidate the structure of the glasses over the whole glass-forming region. It was concluded that the structure is based on randomly distributed $AsSe_{3/2}$ and $SbSe_{3/2}$ trigonal pyramids bridged by common selenium atoms and corresponds to the transition structure between a "random covalent network model" (RCNM) and a "chains crossing model" (CCM).

1. Introduction

Chalcogenide glasses are a family of semiconducting materials that have been studied extensively, particularly for their application in infrared optics [1]. Ternary As-Sb-Se glasses were widely studied in the 1980s and 1990s and were recently "rediscovered" owing to their application for rewritable optical storage, e.g., [2,3]. Understanding the structure of these materials is currently in the spotlight.

The phase diagram of the As_2Se_3-Sb_2Se_3 pseudo-binary system, showing that this stoichiometric system exhibits simple eutectic behavior, was presented by Berkes and Myers in a study of phase relations and liquid structure in the system As-Sb_2Se_3-Se [4]. The authors do not state the exact eutectic composition, but based on the presented phase diagram, it can be estimated to be approx. 11 mol.% Sb_2Se_3. The eutectic temperature was found to be 363 ± 5 °C, which is close to the melting temperature of As_2Se_3, $T_{ons.}$= 370 °C. Platakis and Gatos studied the devitrification kinetics in an $(As_2Se_3)_{100-x}(Sb_2Se_3)_x$ system

using either illumination by a 450 W xenon lamp or slow cooling of the melt. From melts with low Sb contents, the monoclinic As_2Se_3 phase was found to crystallize, whereas the orthorhombic Sb_2Se_3 phase crystallizes for Sb-rich melts [5]. Das et al. [6] investigated the thermodynamic and kinetic behavior of $(As_2Se_3)_{100-x}(Sb_2Se_3)_x$ alloys. They noticed that the glass transition temperature increases in the range 198 to 202 °C with increasing Sb_2Se_3 concentration, and the crystallization rate decreases. In addition to the glass transition, Sawan et al. [7] studied the electrical properties of As-Sb-Se glasses and found that Sb can be added to As_2Se_3 in amounts of up to approximately 19 at.% to preserve the glassy state. Kato et al. reported the thermal properties and structure of As-Sb-Se and As-Sb-S glasses [8,9] and the far-infrared reflectivity and Raman spectra of As-Sb-Se and As-Sb-S glasses [10]. They observed two dominant IR modes corresponding to ($AsSe_{3/2}$) and ($SbSe_{3/2}$) pyramidal units. The infrared intensity of the ($SbSe_{3/2}$) unit was found to be more than twice as strong as that of the ($AsSe_{3/2}$) unit. Mahadevan, Girindhar and Singh [11] intensively studied the calorimetric properties of As-Sb-Se glasses. In one of the most recent papers on As-Sb-Se glasses, Deli et al. [12] correlated the glass transition temperature with the optical gap and observed that the optical gap increases when T_g rises. From structural analyses published in the literature [13-16], ^{77}Se MAS NMR appears to be a very significant tool for the structural description of selenium-containing glasses, notwithstanding a low ^{77}Se sensitivity resulting from its low natural abundance (7.58 %) and long longitudinal relaxation time (between 300 and 600 s [17-19]). The obtained results have confirmed the validity of the chain-crossing model for As_xSe_{1-x} glasses for compositions rich in Se ($0<x<0.4$). Freitas et al. [20] studied As-Se-S glasses using Raman spectroscopy. They reported the presence of mixed pyramidal $AsSe_{3-x}S_x$ units for all x. The existence of these units precludes a phase separation in the studied glasses. G. Delaizir

et al. [21], using wide-angle X-ray scattering and ^{77}Se MAS NMR, observed that the progressive introduction of tellurium in $As_3Se_{(7-x)}Te_x$ glasses induces breakage of Se-Se bonds and formation of mixed pyramidal $AsSe_{(3-x)}Te_x$ units. Using infrared reflectance spectroscopy, Kamitsos et al. [22] studied the structure of the same pseudo-binary stoichiometric system of the present study but based on sulfur. A glass structure formed by a random distribution of trigonal ($AsS_{3/2}$) and ($SbS_{3/2}$) pyramidal units bridged by sulfur atoms was proposed. Glotova and coworkers [23] studied nuclear quadrupole resonance (NQR) and electron spin resonance (ESR) of $(As_2Se_3)_{0.78}(Sb_2Se_3)_{0.22}$, $(As_2Se_3)_{0.75}(Sb_2Se_3)_{0.25}$, and $(As_2Se_3)_{0.5}(Sb_2Se_3)_{0.5}$ glasses and identified two ^{121}Sb-NQR lines and two ^{75}As-NQR lines. Based on the analysis of the ESR results, they suggested the presence of hole-conductivity centers localized on chalcogen atoms and conduction electron centers localized on the arsenic atoms.

The aim of the present study is thermoanalytical and structural characterization by Raman and ^{77}Se NMR of $(As_2Se_3)_{100-x}(Sb_2Se_3)_x$ stoichiometric glasses (or, in rewritten form, an $As_{(40-2x/5)}Sb_{2x/5}Se_{60}$ system) for x covering a maximal possible glass-forming range. Differential scanning calorimetry (DSC) in conventional and StepScan DSC modes, XRD, Raman scattering and ^{77}Se MAS NMR are used. Because Sb_2Se_3 bulk glass cannot be prepared by melt quenching, the Sb_2Se_3 thin film must be used as the border compound, x = 100. In particular, chemometric analysis techniques will be used to interpret the Raman and ^{77}Se MAS NMR data that are poorly resolved.

2. Experimental

2.1 Sample preparations

Bulk samples of $(As_2Se_3)_{100-x}(Sb_2Se_3)_x$ for x=0, 5, 10, 20, 30, 40, 50, 60, 70 and 100 (polycrystalline Sb_2Se_3 for thin film deposition) were prepared by the melt quenching technique from 5N purity elements. The quartz ampoules with appropriate amounts of elements with a total weight of 3 g were evacuated and sealed. Syntheses were performed in a rocking furnace at 850 °C/24 h. Ampoules with glass-forming melts were quenched in the cold water.

An Sb_2Se_3 thin film with a thickness of ~0.9 μm was deposited from a Ta boat with a preliminary calculated amount of polycrystalline Sb_2Se_3 sample. The layers were deposited by thermal evaporation at a deposition rate of 0.7–0.8 nm/s on substrates from the microscopic glass.

2.2 Experimental techniques

XRD analysis of as-quenched glasses and the samples after DSC scans were performed using a D 8 Advance diffractometer (Bruker) using CuKα radiation , λ = 1.54178 Å, from 5.000° to 65.000° with a step of 0.020 ° and a step time of 15.0 s. Diffractograms were compared with the database PDF-4+; version 2014, Joint Committee on Powder Diffraction Standards, Int. Centre of Diffraction. Data, Swarthmore, PA, USA. The accuracy of the determination of the diffraction lines was ± 0.02^o of 2Θ. To assign standards, accordance ± 0.05 ° of 2Θ was used.

Energy-dispersive X-ray spectroscopy (EDX) employing a Jeol JSM 5500LV and a scanning electron microscope (accelerating voltage 20 kV) was used determine the chemical composition. The experimental error of analysis was ±1 at. %.

A Diamond differential scanning calorimeter (DSC) (Perkin-Elmer) was used for the thermoanalytical study. Instruments were both temperature and enthalpy calibrated

with the help of In and Zn standards; the correctness of the measurement of isobaric heat capacity was verified by measuring the monocrystalline corundum standard. Measurements were carried out under nitrogen purging. Samples (approximately 10 mg) were encapsulated in aluminum pans, and an empty pan was used as a reference. The accuracy of the temperature determination is better than ±0.5 °C. The glass transition temperature, T_g, determined as a temperature at the ΔC_P midpoint, and the isobaric heat capacities, $C_p^{glass}(T_g)$ and ΔC_P, were measured with the help of the stepwise StepScan DSC technique. The temperature dependence of both the isobaric heat capacity and enthalpic changes of kinetic events were obtained. StepScan DSC measurements were carried out in the temperature range of 50 to 450 °C with a temperature step of 1 °C, a heating rate of 10 °C/min, an isotherm duration 60 s and a maximal heat flow change allowed before next step of ±0.005 mW. For more details on this technique, see [24,25]. The crystallization of glass-forming melts was studied by heating in conventional DSC mode with a heating rate of 10 °C/min.

Raman scattering measurements were carried out using an FTIR spectrometer IFS - 55 with a Raman attachment FRA 106 (both Bruker) and a liquid nitrogen-cooled germanium detector. A Nd:YAG laser (1064 nm) was used for scattering excitation. Raman spectra were recorded at room temperature as an average of 250 scans with a resolution of 1 cm^{-1}. Experimental spectra were reduced according the relation proposed by Shuker and Gammon [26].

The ^{77}Se MAS NMR spectra were recorded at room temperature on an Avance 300 Bruker spectrometer operating at 57.28 MHz with a 4 mm MAS probe. The spectra were recorded with a spinning speed of 15 kHz, simultaneously averaging the chemical shift and reducing the homonuclear dipolar interaction between Se atoms. A Hahn spin echo

sequence was applied to refocus the magnetization. Fourier transformation was performed on the entire magnetization to improve the signal-to-noise ratio and avoid any distortion of the baseline. The processing and acquisition parameters were as follows: 3.5 μs π/2 pulse duration (7 μs for the π pulse), 300 s recycle time, 1 MHz spectral width, time domain 1 K, 3000 accumulated scans. The external reference used for the chemical shift was a saturated solution of Me_2Se in $CDCl_3$ [27].

Chemometric analysis, specifically, multivariate curve resolution (MCR), included in the Solo+MIA chemometric software (Eigenvector Research Inc., USA) was used for analysis of the sets of Raman and ^{77}Se MAS NMR spectra. The objective of MCR is to extract concentration profiles and pure component spectra. It is expected that data can be decomposed as nonnegative concentrations times nonnegative spectra, which is fulfilled in our case.

3. Results and discussion

3.1 Thermoanalytical study

EDX analysis confirmed, within the margins of the experimental error ± 1%, the nominal compositions of all bulk samples and of the Sb_2Se_3 thin film. XRD did not find diffraction peaks for crystals either in the samples $(As_2Se_3)_{100-x}(Sb_2Se_3)_x$ for x = 0–50 or in the Sb_2Se_3 thin film. However, bulk samples for x > 50 were partially crystallized and thus were excluded from the study.

Although XRD analysis verified that the Sb_2Se_3 thin film is non-crystalline, neither conventional DSC nor StepScan DSC could find its glass transition [28]. This is not an isolated case for thin films; in fact, a glass transition was also not observed for, e.g.,

$Ge_2Sb_2Te_5$ [29], $Ge_4Sb_1Te_5$, $Ge_1Sb_2Te_4$, $Ge_2Sb_2Te_5$ and $Ag_{0.055}In_{0.065}Sb_{0.59}Te_{0.29}$ thin layers [30].

Concerning bulk glasses, compositional dependence of the glass transition temperature, T_g, the isobaric heat capacity of glass at T_g, $C_p^{glass}(T_g)$, and the isobaric heat capacity difference at the glass transition, ΔC_P, were obtained by StepScan DSC, and the results are summarized in Figs. 1 and 2. First, only one glass transition was found for each glass, proving that no segregation occurred, and thus, T_g, $C_p^{glass}(T_g)$ and ΔC_P can be correlated with nominal composition.

The glass transition temperature rises slightly but clearly from 184 °C for x=0, i.e., As_2Se_3, to 189 °C for x = 50 as the Sb_2Se_3 content increases (Fig. 1). This behavior is similar to the results obtained by Das and coauthors [6], but the glass transition temperatures obtained in this study are lower by approximately 9 °C. The chemical compositions of all glass samples agree with their nominal compositions; consequently, this difference relates to the StepScan DSC technique used for our measurements. This technique separates kinetic effects and thus shifts T_g to a lower temperature for each composition [24]. The small increase in T_g when 50% of the composition is changed can be explained by the fact that the bond energies of As-Se (1.80 eV) and Sb-Se (1.86 eV) are close to each other [31] and the geometry of the basic structural units are the same—trigonal pyramids. However, substitution of arsenic by antimony causes a decrease in the isobaric heat capacity at the glass transition temperature, $C_p^{glass}(T_g)$, for x between 5 and 10 mol.% of Sb_2Se_3 (Fig. 2). This can be understood considering the greater mass of antimony by a factor of 1.6 compared to that of arsenic and therefore the lower vibrational energy. However, compositional dependence of ΔC_P changes slightly over the whole glass-forming region, maximally by 0.016 J/(g.K) (Fig. 2). This finding agrees well with the facts that the

only structural unit over the whole compositional range is a trigonal pyramid and that the bond energies of As-Se and Sb-Se are very similar. Thus, the changes in the vibrational amplitudes during the glass transition, i.e., the changes between glass and its undercooled melt at T_g, are only slightly compositionally dependent.

To obtain information on the undercooled melt stability, all bulk glasses were studied during heating by conventional DSC. First, one and then two broad crystallization peaks were observed depending on the content of Sb_2Se_3. The temperature of the second exothermic peak (this one at a lower temperature) decreases with increasing antimony content while the peak becomes sharper (Fig. 3). Thus, the temperature range of undercooled melt stability decreases, and consequently, the glass-forming ability by melt cooling decreases. XRD analyses indicate that for $x \leq 20$, only As_2Se_3 crystallized, whereas when $x > 20$, both As_2Se_3 and Sb_2Se_3 undergo crystallization. These results agree with the eutectic phase diagram of the studied binary stoichiometric system [4]. For $x \leq 10$, the crystallization of arsenic triselenide agrees with the phase diagram because the eutectic composition is close to 11 mol.% Sb_2Se_3. However, for $x > 10$, the stoichiometric compound able to crystallize should be antimony triselenide; however, surprisingly, crystals of both stoichiometric selenides were found by XRD. This behavior can be understood by considering that the addition of Sb_2Se_3 to As_2Se_3 has a radical effect on the viscosity of the melt and the crystallization kinetics of As_2Se_3 crystals [4]. Pure As_2Se_3 is extremely viscous, and crystals grow very slowly, whereas at a composition of 20 mol.% Sb_2Se_3, devitrification with the relatively rapid formation of As_2Se_3 crystals is relatively easy.

Regarding the endothermic peaks, their temperature decreases from the melting temperature of As_2Se_3 to the eutectic temperature for the samples with x lower than 20; for

higher values, they remain independent of chemical composition (Fig. 3). Remarkably, a low area of the As_2Se_3 melting peak (low enthalpy change) is related to the extreme viscosity of the As_2Se_3 melt, as mentioned in the previous paragraph. A compositional peak shift observed for lower concentrations of Sb_2Se_3 ($x < 20$) corresponds to the shift of the dissolving peak of crystalline As_2Se_3 in the melt. However, the eutectic temperature is very close to the melting temperature of As_2Se_3; thus, the peaks of eutectic melting and the ensuing dissolution of As_2Se_3 merge into a single broader peak. This merging peak shifts to the eutectic temperature with increasing content of Sb_2Se_3. For samples with $x = 20$ and higher, i.e., samples with over-eutectic contents of Sb_2Se_3, only eutectic melting is observed in Figure 3 because the melting temperature of Sb_2Se_3 (590 °C) is out of the measurement range. Despite this, one can see a part of Sb_2Se_3 dissolving on the DSC traces for $x = 20$ and 30.

3.2 Structural study—Raman spectroscopy and ^{77}Se MAS NMR

The main feature of the set of Raman spectra is a broad band with the maximum more or less monotonically shifting from 233 to 191 cm^{-1} and a decreasing shoulder at approx. 239 cm^{-1} when the content of Sb_2Se_3 increases (Fig. 4). Based on the realistic supposition that the structural units of studied glasses are $AsSe_{3/2}$ and $SbSe_{3/2}$ trigonal pyramids only [8,9,10], the compositional dependence of the Raman spectra simply reflects the fact that one structural unit replaces another isostructural one. Stemming from the fact that only one glass transition was observed for each type of glass, one must suppose selenium bridges (=As-Se-Sb=) to be an interconnection of arsenic- and antimony-based trigonal pyramids. Using multivariate curve resolution (MCR), chemometric analysis of the set of Raman spectra showed that the studied glasses can be well

characterized by the linear combination of the three independent components (see Fig. 5). The variance captured by the MCR model is better than 99 %. Two of the resolved components on the inset of Fig. 5 correspond to the border compositions, x = 0 (Comp. 1) and x = 100 (Comp. 2), and their vibrational modes reflect the fact that the 3D structure is composed only of $AsSe_{3/2}$ and/or $SbSe_{3/2}$ trigonal pyramids surrounded by the same structural units; from another perspective, this means that vibration modes correspond to vibrations of either =As-Se-As= or =Sb-Se-Sb= bridges. The third resolved component (Comp. 3) corresponds to the 3D structure of periodically alternating $AsSe_{3/2}$ and $SbSe_{3/2}$ pyramids; this corresponds to a composition of x = 50, and the vibrational modes are modes of =As-Se-Sb=. A comparison of experimental and reconstructed spectra and residuals is shown in Fig. 6. We must stress that because the system under study is pseudobinary and stoichiometric, MCR analysis was also tested for only two components, but reconstruction of experimental spectra was practically impossible; the error reached almost 40 %.

To obtain the compositional dependence of three possible selenium bridges, ^{77}Se MAS NMR spectra were recorded for all $(As_2Se_3)_{100-x}(Sb_2Se_3)_x$ bulk glasses (x = 0 to 50) and for amorphous Sb_2Se_3 thin films (Fig. 7). Owing to the low abundance of ^{77}Se and its long longitudinal relaxation time, the signal-to-noise ratio is poor. The glassy network of As_2Se_3 (x = 0) composed of Se-connected $AsSe_{3/2}$ pyramids gives rise to a single line centered around 390 ppm relating to an As-Se-As unit [13-14]. The initial line of As_2Se_3 becomes increasingly asymmetric when the substitution of arsenic by antimony gradually increases. Thus, the broad spectrum encompasses a growing component at a lower chemical shift corresponding to the chemical shift of the ^{77}Se that is related to Sb-Se-As and maybe to Sb-Se-Sb for the richer composition in Sb. Using MCR, the chemometric

analysis of the set of ^{77}Se MAS NMR spectra has also been performed, and three different selenium sites and the compositional dependencies of their scores were identified (Fig. 8). The detection of these three contributions is consistent with the twofold coordination state of selenium in chemistry. As in the case of Raman spectra, the model captures more than 99 % of the variance of experimental data. Using the MCR results, the experimental spectra were reconstructed (see Fig. 9). Based on the chemical composition dependence of selenium site intensities, the first site characterized by a chemical shift of 393 ppm is related to selenium in the =As-Se-As= structure, which is in full agreement with previous studies [14-17]. At the opposite side of the chemical shift scale, the line at -19 ppm is quite logically assigned to =Sb-Se-Sb= sequences. Thus, the third site, characterized by an intermediate chemical shift value of 206 ppm, is ascribed to the =As-Se-Sb= structural unit. The compositional trend of the fractions of these three sites obtained by MCR, Fig. 8, is basically the same as that obtained by the aforementioned analysis of Raman spectra (Fig. 5). The studied system can be shown as a solid solution formed by randomly distributed trigonal pyramids of $AsSe_{3/2}$ and $SbSe_{3/2}$ interconnected by mutual single-selenium bridges. This view agrees with the structure of $(As_2S_3)_{100-x}(Sb_2S_3)_x$ proposed on the basis of infrared reflectance spectroscopy, [22].

The fraction of structural units obtained by both Raman and NMR spectroscopy for each studied composition, Figs. 5 and 8, were averaged, and these mean values were compared with the two structural models, namely, a "chains crossing model" (CCM) and a "random covalent network model" (RCNM) (Fig. 10), for deeper elucidation of the structure of the studied glasses. The result shows that structure of glasses is "halfway" between these structural models. This is surprising because the current system is stoichiometric and pseudobinary and the As-Se and Sb-Se bond energies are similar; thus, no bonding partner

of selenium should be preferred. Therefore, the structure of the glasses should be close to the ideal solution, and the RCN model should be suitable for its description. However, the deviation toward a CCM shows that =As-Se-Sb= bridges are somewhat more preferred. Entropy may have been responsible, but this has yet to be elucidated.

4. Conclusions

The basic thermoanalytical characteristics and structure of $(As_2Se_3)_{100-x}(Sb_2Se_3)_x$ bulk glasses covering the whole glass-forming region (x = 0–50) and Sb_2Se_3 thin films (x = 100) used as the second border composition were studied by DSC, StepScan DSC and both Raman and ^{77}Se MAS NMR spectroscopies.

The glass transition temperature was found to increase slightly from 184 to 190 °C when the content of Sb_2Se_3 increases from x = 0 to 50. The glass transition of Sb_2Se_3 was not found. At the same time, when the glass transition increases, the isobaric heat capacity of glasses, which is measured at the glass transition onset on the glass side of the glass transition, decreases because arsenic atoms are replaced by antimony, which has a significantly higher atomic mass. Conversely, the compositional dependence of the change of isobaric heat capacity during glass transition is small, showing that structural changes between glasses and their undercooled melts are compositionally nearly independent. The undercooled melts are unstable and undergo crystallization when heated; for $x \leq 20$, only arsenic triselenide crystallizes; for higher x, both As_2Se_3 and Sb_2Se_3 crystalline phases were identified.

Raman spectroscopy, ^{77}Se MAS NMR and especially chemometric analyses of compositional dependencies of both sets of spectra showed that the structure of the glasses over the whole glass-forming region is based on randomly distributed $AsSe_{3/2}$ and $SbSe_{3/2}$

trigonal pyramids bridged by common selenium atoms at the vertices of the pyramids. These findings indicate that the structure of glasses of a pseudobinary stoichiometric system substantially corresponds to the transition structure between models known as a "random covalent network model" (RCNM) and a "chains crossing model" (CCM). These conclusions are rather in agreement with previous works carried out in binary selenide systems, As_xSe_{1-x} [14, 16, 17] and Ge_xSe_{1-x} [15, 18, 19]. Moreover, the present study shows that chemometric analysis is a very fruitful way to obtain some structural information from poorly resolved solid-state Raman and NMR spectra. To the best of our knowledge, this is the first time that such analyses have been carried out in that frame.

5. Literature

[1] A. Zakery, S.R. Elliot, Optical properties and applications of chalcogenide glasses. J. Non-Cryst. Solids 330 (2003) 1-13.

[2] V.I. Mikla, I.P. Mikhalko, V.V. Mikla, Laser-induced amorphous-to-crystalline phase transition in Sb_xSe_{1-x} alloys, Mat. Sci. Eng. 83 (2001) 74-78.

[3] A. Kapoutsis, E.I. Kamitsos, I.P. Couleac, M.S. Iovu, Physics and Applications of Non-Crystalline Semiconductors in Optoelectronic, Kluwer Academic Publisher, Netherland, A. Andriesh, M. Bertoletti editors, 1997.

[4] J.S. Berkes, M.B. Myers, Phase relations and liquid structure in the system As-Sb_2Se_3-Se, J. Electrochem. Soc. 118 (1971) 1485-1491.

[5] N.S. Platakis, H.C.Gatos, Devitrification characteristic of the semiconductor system (1-x)As_2Se_3 xSb_2Se_3, Solid State Sci. Tech. 119 (1972) 914-918.

[6] G.C. Das, N.S. Platakis, B. Bever, A thermodynamic and kinetic investigation of amorphous (1-x)As_2Se_3 xSb_2Se_3 alloys, J. Non-Cryst. Solids 15 (1974) 30-44.

[7] Y. Sawan, F.G. Wakim, M. El-Gabaly, M.K. El-Rayess, Study of the region of glass formation and electrical properties of the As-Se-Sb system, J. Non-Cryst Solids 41 (1980) 319-325.

[8] M. Kato, S. Onari, T. Arai, Thermal properties and structure of As-Sb-Se and As-Sb-S glasses, Jpn. J. Appl. Phys. 20 (1981) 2013-2017.

[9] M. Kato, S. Onari, T. Arai, Study of structure of As-Sb-Se and As-Sb-S glasses, Jpn. J. Appl. Phys. 22 (1983) 1392-1399.

[10] S. Onari, M. Kato, T. Arai, Two fonon vibration spectra of amorpnous As-Sb-Se and As-Ab-S, J. Non-Cryst. Solids 95-96 (1987) 287-292.

[11] S. Mahadevan, A. Girindhar, A.K. Singh, Calorimetric measurements on As-Sb-Se glasses, J. Non-Cryst. Solids 11 (1986) 88-92.

[12] M.L. Deli, D.H. Boigny, G. Kra, The structural properties of Sb_2Se_3-As_2Se_3 and Sb_2STe_3-As_2Se_3 glasses, J. Non-Cryst. Solids 10 (2010) 59-65.

[13] B. Bureau, J. Troles, M. LeFloch, F. Smektala, G. Silly, J. Lucas, Solid state ^{77}Se NMR investigation on arsenic-selenium glasses and crystals, Solid State Sci. 5 (2003) 219–224.

[14] M. Deschamps, C. Roiland, B.Bureau, G.Yang, L. Le Poll, D. Massiot, ^{77}Se solid-state NMR investigation on As_xSe_{1-x} glasses using CPMG acquisition under MAS, Solid State Nuclear Mag. Res. 40 (2011) 72–77.

[15] C. Derric, D.C. Kaseman, I. Hung, Z.H. Gan, S. Sen, Observation of a continuous random network structure in Ge_xSe_{100-x} Glasses: Results from high-resolution ^{77}Se MATPASS/CPMG NMR spectroscopy, J. Phys. Chem. B 117 (2013) 949-954.

[16] D.C. Kaseman, I. Hung, Z.H. Gan, B. Aitken, S. Currie, S. Sen, Structural and topological control on physical properties of arsenic-selenide glasses, J. Phys. Chem. B 118 (2014) 2284-2293.

[17] K. Sykina, G.Yang, C. Roiland, L. Le Polles, E. Le Fur, C.J. Pickard, B. Bureau, E. Furet, ^{77}Se solid-state NMR of As_2Se_3, As_4Se_4 and As_4Se_3 crystals: a combined experimental and computational study, Phys. Chem. Chem. Phys. 15 (2013) 6284-6292.

[18] M. Deschamp, C. Genevois, S. Cui, C. Roiland, L. Lepollès, E. Furet, D. Massiot, B. Bureau, Structure of Arsenic Selenide Glasses Studied by NMR: Selenium Chain Length Distributions and the Flory Model, J. Phys. Chem. C 119 (2015) 11852-11857.

[19] K. Sykina, B. Bureau, L. Le Polles, C. Roiland, M. Deschamp, C.J. Pickard, E. Furet, A combined ^{77}Se NMR and molecular dynamics contribution to the structural understanding of the chalcogenide glasses, Phys. Chem. Chem. Phys. 16 (2014) 17975-17982.

[20] J.A. Freitas, U. Strom, D.J. Treacy, Raman scattering of the mixed chalcogenide glass system $As_2S_xSe_{3-x}$, J. Non-Cryst Solids 59-60 (1983) 875-878.

[21] G. Delaizir, M. Dussauze, V. Nazabal, P. Lecante, M. Dollé, P. Rozier, E.L. Kamitsos, P. Jovari, B. Bureau, Structural characterizations of As-Se-Te glasses. J. Alloys Comp. 509 (2011) 831–836.

[22] E.I. Kamitsos, J.A. Kapoutsis, I.P. Culeac, M.S. Iovu, Structure and bonding in As-Sb-S glasses by infrared reflectance spectroscopy, J. Phys. Chem. 101 (1997) 1061-11067.

[23] O. Glotova, I. Korneva, N. Sinyavsky, B. Dobosz, R. Krzyminiewski, M. Jadzyn, M. Ostafin, B. Nogaj, Study of As-Sb-Se chalcogenide glasses by NQR and EPR spectroscopy methods, Central European J. Phys. 9 (2011) 387-391.

[24] J. Holubová, Z. Černošek, E. Černošková, The study of the glass transition by the StepScan DSC technique, J. Optoelectron. Adv. Mater. 7 (2005) 2671-2676.

[25] Z. Černošek, J. Holubová, E. Černošková, Capability of conventional differential scanning calorimetry, temperature modulated DSC and StepScan DSC for the glass transition phenomenon study, Optoelectron. Adv. Mater. Rapid Commun. 1 (2007) 277-280.

[26] R. Shuker, R.W. Gammon, Raman scattering selection-rule breaking and the density of states in amorphous materials, Phys. Rev. Lett. 25 (1970) 222-226.

[27] H. Duddeck. Selenium-77 Nuclear Magnetic Resonance Spectroscopy, Prog. Nucl. Magn. Reson. Spectrosc. 27 (1995) 1-23.

[28] E. Černošková, R. Todorov, Z. Černošek, J. Holubová, L. Beneš, Thermal properties and the structure of amorphous Sb_2Se_3 thin film, J. Therm. Anal. Calorim. 118 (2014) 105-110.

[29] J. Orava, A.L. Greer, B. Gholipour, D.W. Hewak, C.E. Smith, Characterization of supercooled liquid $Ge_2Sb_2Te_5$ and its crystallization by ultrafast-heating calorimetry, Nature Mater. 11 (2012) 279-283.

[30] J.A. Kalb, M. Wuttig, F. Spaepen, Calorimetric measurement of structural relaxation and glass transition temperatures in sputtered films of amorphous Te alloys used for phase change recording, J. Mater. Res. 22 (2007) 748-754.

[31] L. Tichý, H. Tichá, Covalent bond approach to the glass transition temperature of chalcogenide glasses, J. Non-Cryst. Solids 189 (1995) 141-146.

Figure captions

Fig. 1 Compositional dependence of the glass transition temperature.

Fig. 2 Compositional dependence of the isobaric heat capacity of glass at the beginning of the glass transition region and difference of the isobaric heat capacity during glass transition.

Fig. 3 DSC traces of bulk glasses. For details, see the text.

Fig. 4 Reduced Raman spectra of $(As_2Se_3)_{100-x}(Sb_2Se_3)_x$ glasses ($0 \leq x \leq 50$) and thin films ($x = 100$).

Fig. 5 Compositional dependence of the scores on components for reconstruction of experimental Raman spectra by means of their linear combination obtained by MCR analysis of set of experimental spectra of $(As_2Se_3)_{100-x}(Sb_2Se_3)_x$ glasses ($0 \leq x \leq 50$) and film ($x = 100$). Inset: Components resolved by MCR analysis.

Fig. 6 Experimental (black) and reconstructed (red) Raman spectra and residuals (blue) obtained using the MCR model.

Fig. 7 ^{77}Se MAS NMR spectra of $(As_2Se_3)_{100-x}(Sb_2Se_3)_x$ glasses ($0 \leq x \leq 50$) and thin film ($x = 100$).

Fig. 8 Compositional dependence of the scores on components for reconstruction of experimental ^{77}Se MAS NMR spectra by means of their linear combination obtained by MCR analysis of a set of experimental spectra of $(As_2Se_3)_{100-x}(Sb_2Se_3)_x$ glasses ($0 \leq x \leq 50$) and film ($x = 100$). Inset: Components resolved by MCR analysis.

Fig. 9 Experimental (black) and reconstructed (red) ^{77}Se MAS NMR spectra and residuals (blue) obtained using the MCR model.

Fig. 10 Comparison of the MCR results with RCNM and CCM structural models. For details, see the text.

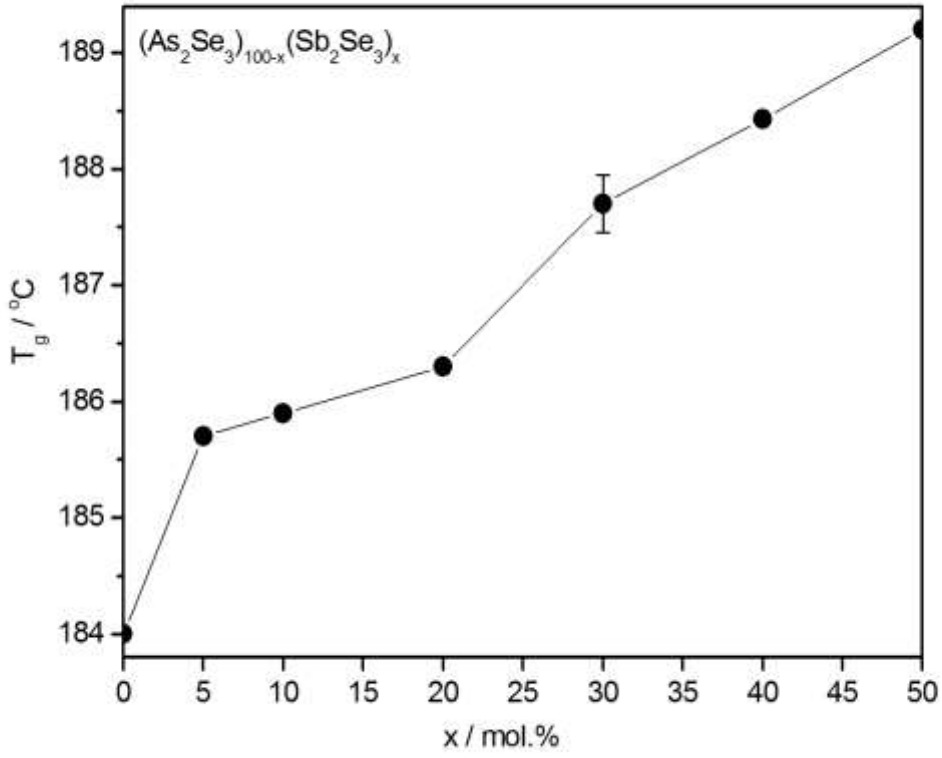

(As2Se3)100-x(Sb2Se3)x
Tg / °C
x / mol.%
189
188
187
186
185
184
0
5
10
15
20
25
30
35
40
45
50

Fig. 1

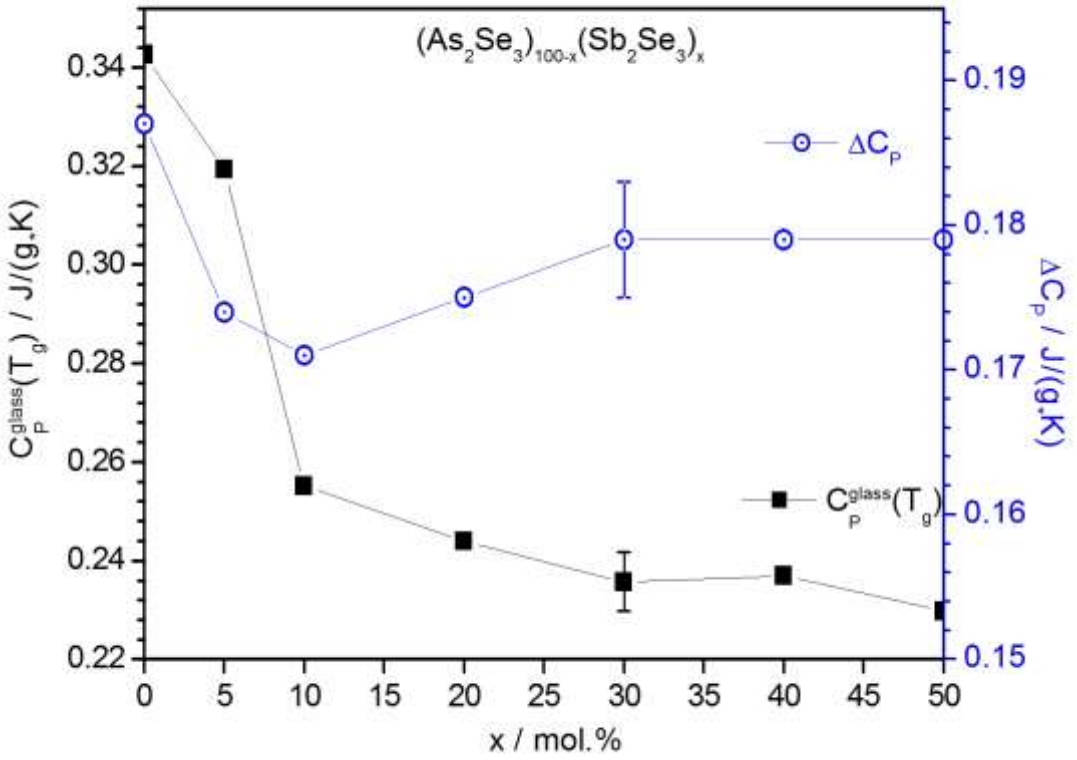

(As2Se3)100-x(Sb2Se3)x
ΔCP
CPglass(Tg)
CPglass(Tg) / J/(g.K)
ΔCp / J/(g.K)
x / mol.%
0.34
0.32
0.30
0.28
0.26
0.24
0.22
0.19
0.18
0.17
0.16
0.15
0
5
10
15
20
25
30
35
40
45
50

Fig. 2

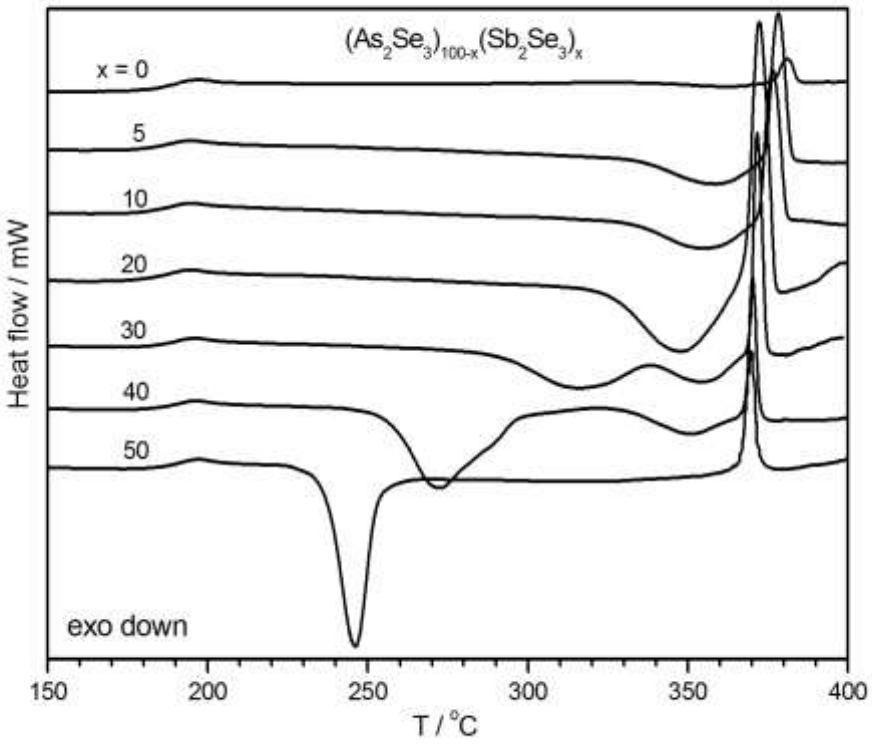

(As2Se3)100-x(Sb2Se3)x
x = 0
5
10
20
30
40
50
Heat flow / mW
exo down
150
200
250
300
350
400
T / °C

Fig. 3

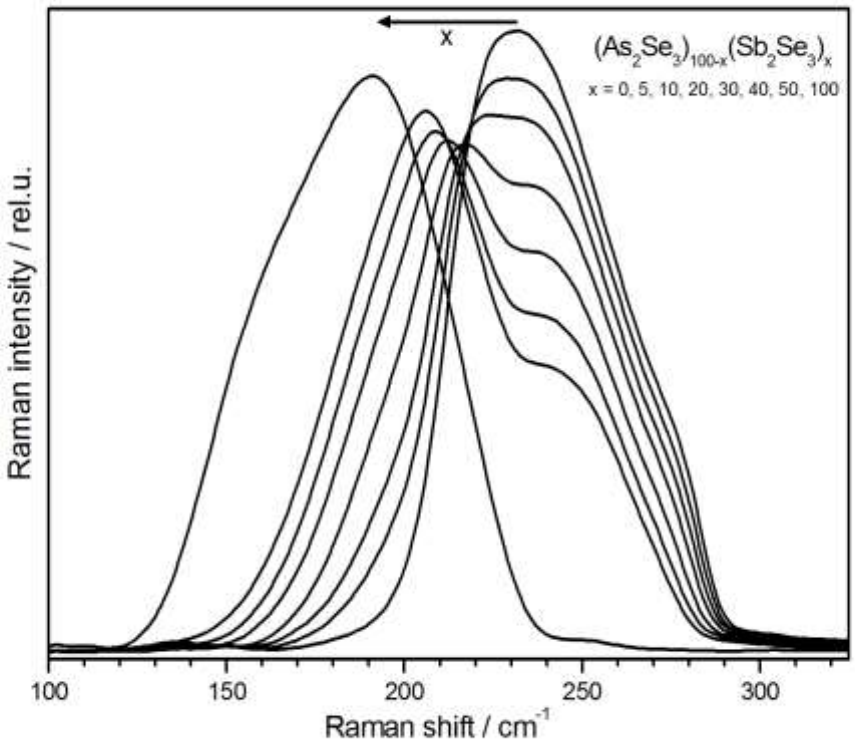

x
$(As_2Se_3)_{100-x}(Sb_2Se_3)_x$
x = 0, 5, 10, 20, 30, 40, 50, 100
Raman intensity / rel.u.
100
150
200
250
300
Raman shift / cm^{-1}

Fig. 4

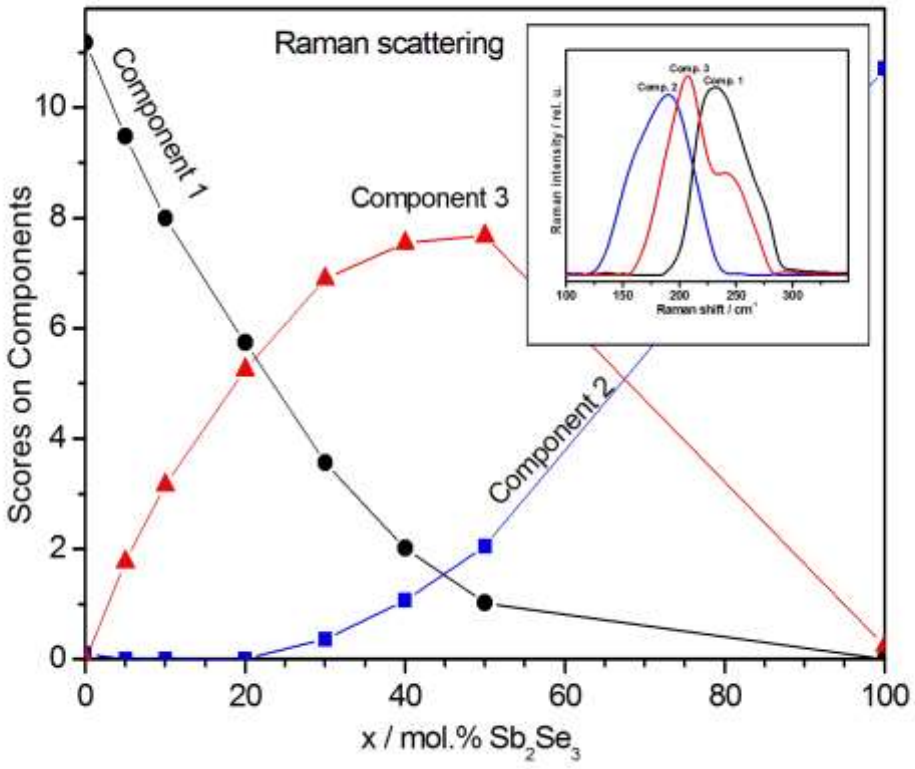

Raman scattering
Component 1
Component 3
Component 2
Scores on Components
x / mol.% Sb2Se3
0
2
4
6
8
10
0
20
40
60
80
100
Comp. 3
Comp. 2
Comp. 1
Raman intensity / rel. u.
100
150
200
250
300
Raman shift / cm-1

Fig. 5

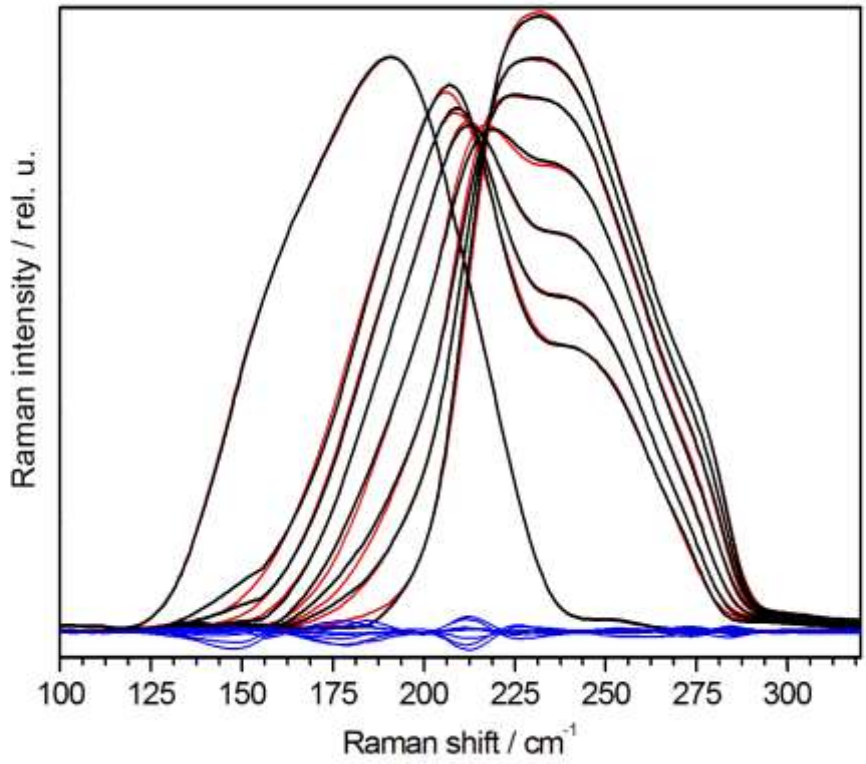

Raman intensity / rel. u.
100
125
150
175
200
225
250
275
300
Raman shift / cm-1

Fig. 6

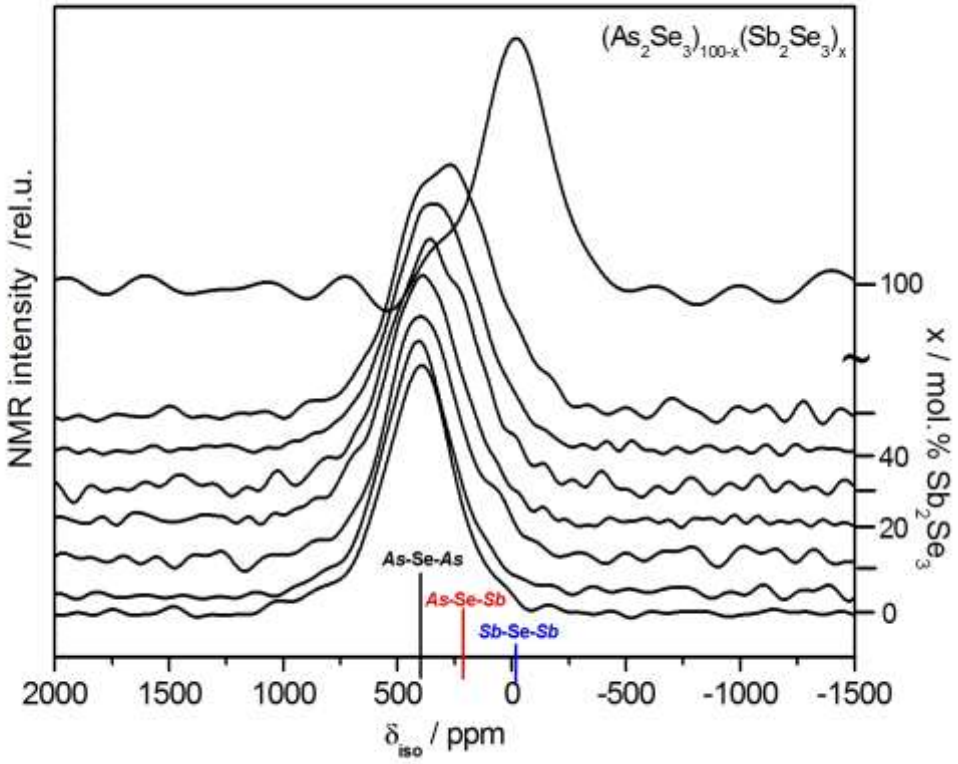

(As2Se3)100-x(Sb2Se3)x
NMR intensity /rel.u.
100
40
20
0
x / mol.% Sb2Se3
As-Se-As
As-Se-Sb
Sb-Se-Sb
2000
1500
1000
500
0
-500
-1000
-1500
δiso / ppm

Fig. 7

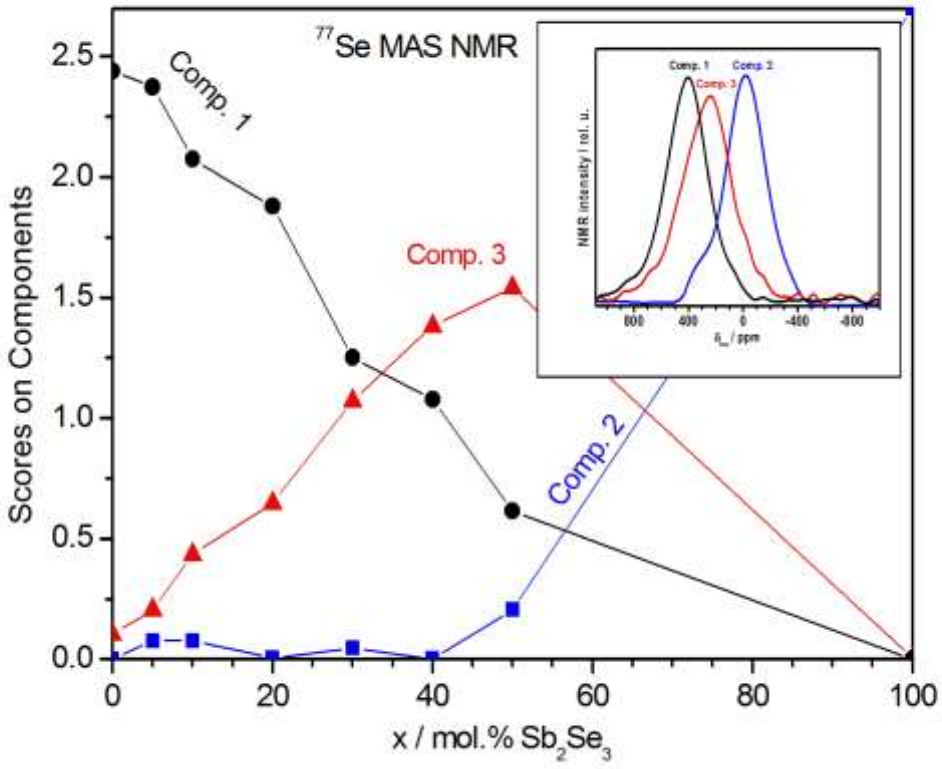

^{77}Se MAS NMR
Comp. 1
Comp. 3
Comp. 2
Scores on Components
x / mol.% Sb_2Se_3
NMR intensity / rel. u.
δ_{iso} / ppm

Fig. 8

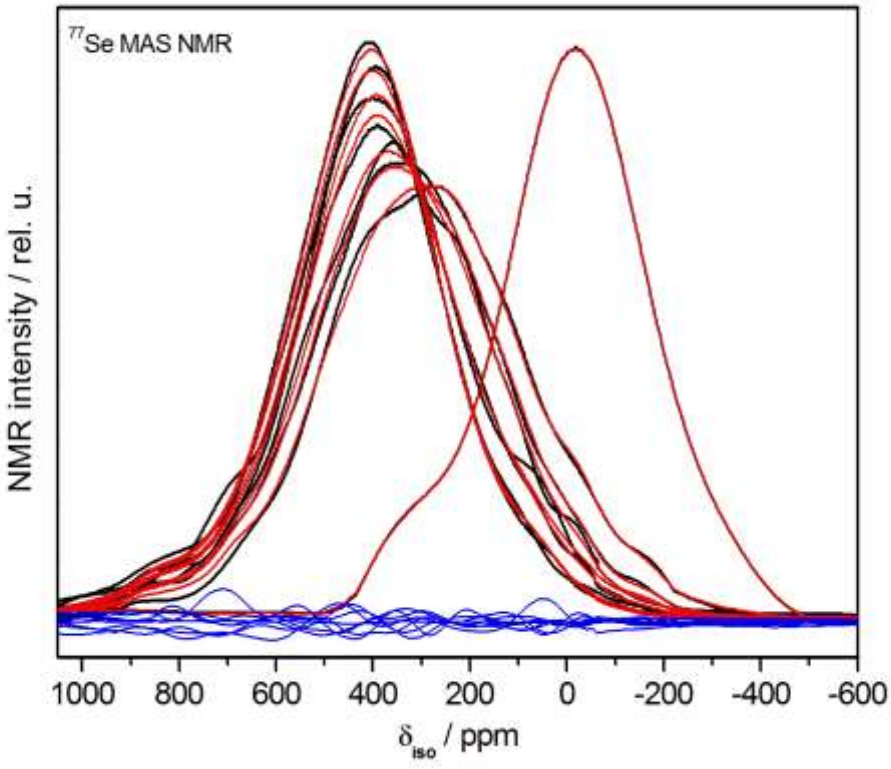

77Se MAS NMR
NMR intensity / rel. u.
1000
800
600
400
200
0
-200
-400
-600
δiso / ppm

Fig. 9

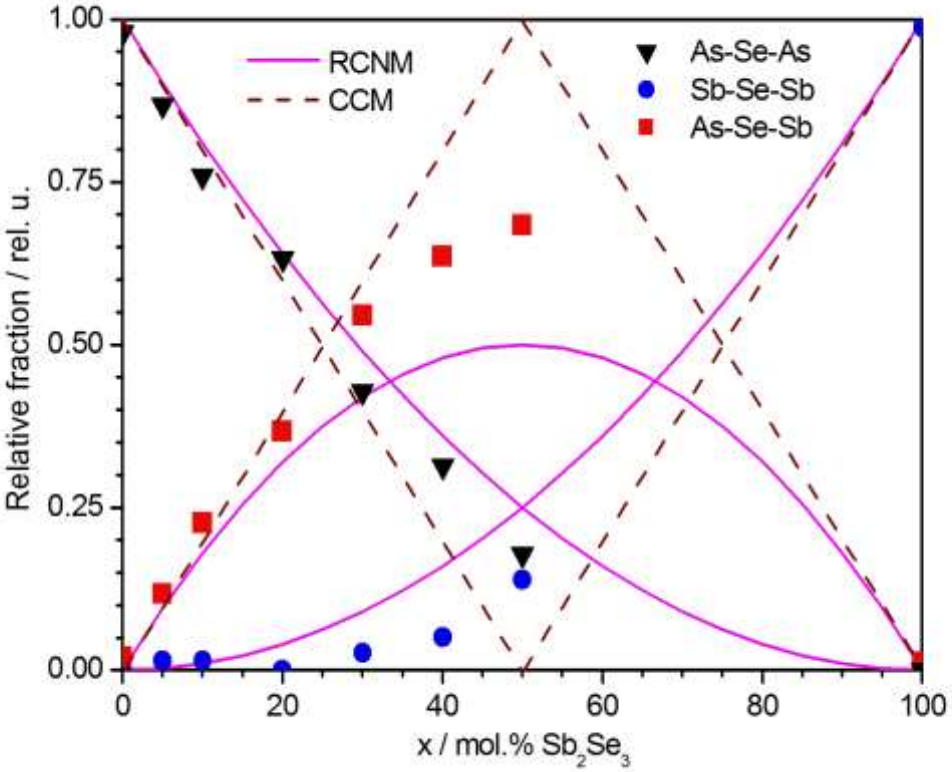

1.00
0.75
0.50
0.25
0.00
Relative fraction / rel. u.
0
20
40
60
80
100
x / mol.% Sb2Se3
RCNM
CCM
As-Se-As
Sb-Se-Sb
As-Se-Sb

Fig. 10